Nigerian Journal of Technology (NIJOTECH)
Vol. 42, No. 2, June, 2023, pp.230 - 235
www.nijotech.com

Print ISSN: 0331-8443
Electronic ISSN: 2467-8821
https://doi.org/10.4314/njt.v42i2.10

SYNTHESIS AND CHARACTERIZATION OF MEHTYLAMMONIUM BISMUTH IODIDE VIA SOLVENT ENGINEERING

B. Abdulkareem[1,*]

[1]Department of Mechanical and Production Engineering, Ahmadu Bello University, Zaria, Nigeria

*corresponding author (Email: ogabello2002@yahoo.com)

Article history: Received 30 December, 2022. Revised 15 March, 2023. Accepted 31 March, 2023. Published 31 July, 2023. *CC BY-NC-ND Licence*

Abstract
Hybrid organic–inorganic halide perovskites (OIHPs) are an emerging class of photovoltaic materials that have gained tremendous attention in the field of optoelectronics. This work aims to investigate the characteristics of bismuth-based halide perovskite via solvent engineering for solar cell application. A bismuth-based organo-inorganic perovskite was synthesized and characterized for solar cell application via solvent engineering using Gamma Butyrolactone (GBL) as the based solvent and enhanced with Methylamine (MA) and acetonitrile (ACN). A solution processing facile method was adopted in the synthesis of the perovskite. The solvent engineering aims to tune its band gap and a remarkable band gap of 1.58eV which is within the range of an ideal band gap (1.5-1.6) required for solar cell application. The XRD micrograph exhibited several narrow sharp peaks which indicated crystallinity formation of the synthesized sample with 86% crystallinity. The FESEM/EDS micrograph indicated nature of the formed crystals and the chemical composition of the sample. A multilayer heptagonal crystal was observed. The TGA result showed that the sample is thermally stable at a temperature of 200^{o}C before degradation occurred.

Keywords: Bismuth, Perovskite, Band gap, Photovoltaic, Optoelectronics.

1.0 INTRODUCTION

A solar cell is a semiconductor device that converts light into electrical energy. The conversion is accomplished by absorbing light and ionizing crystal atoms, thereby creating free, negatively charged electrons and positively charged ions. Solar cell has properties similar to a free electron except that it has the opposite charge. Solar cells can be made from single crystals, crystalline and amorphous semiconductors. Each photon of the light that has a high enough energy to be absorbed by the crystal's atoms will set free an electron hole pairs [1].

The electron and hole are free to move through the lattice in a Brownian motion; however, on average they will never move too far from each other. On the other hand, when they experience an electric field, this will tend to separate the electrons from the holes; the electrons will drift toward the positive pole (the anode), and the positively charged holes will drift toward the cathode [2]. Photo conductors are passive devices; they react to light by changing their electric conductivity. In order to activate them, an external electric power source, such as a battery is required [1]. Solar cell module consists of a transparent conducting glass which serve as the cathode, electron transport layer, light absorbing layer, hole transport layer and the anode. Electron-hole pairs are generated when photon of light impinges on the light absorbing layer. Electrons generated via photovoltaic action are extracted by electron transport layer and then drifted towards the cathode while the photogenerated holes are drifted to the anode via hole transport layer.

Researchers are committed to the development of new materials whose efficiency can exceed the present-day silicon used in solar cell. The recent discovery of methylammonium lead iodide perovskite ($MAPbI_3$) by Miyakasa and his co-workers in 2009 unfolded the photovoltaic effect of organo-inorganic halide perovskite (OIHP) to the scientific community. Hence researchers are currently committed to the discovery of more of such class of material as light absorbing layer. OIHP solar cell discovered by Miyasaka et al in 2009 with a power conversion efficiency (PCE) of 3.8%. Few

years later, the PCE) of OIHP solar cell has reached to 25.7% [3]. This competitive increase in its efficiency has been made possible due to the unique optoelectronic properties of the OIHP [4-7,9] such as direct band gap, high absorption coefficient, and charge transport properties.

However, this remarkable improvement in the power conversion efficiency of OIHP is deterred by the poor air stability of perovskite absorbers. This is basically true for polycrystalline thin films perovskite solar cells because their performance is drastically affected by the shorter diffusion length and high trap state densities [4, 10] However, commercialization of methylammonium lead iodide ($MAPbI_3$) despite its high PCE has been marred due the presence of the lead (Pb) which is toxic to the environment and its instability in air. Hence, this work is focused on synthesis and characterization of lead-free OIHP via solvent engineering with the hope of tuning its band gap for solar cell application.

2.0 MATERIALS AND METHODS

2.1 Materials

All reactants and solvents were of analytical grade and used without purification. Methylamine (CH_3NH_2, 33 wt% in ethanol), hydroiodic acid distilled (HI 57 wt% in water), diethyl ether, bismuth (III) iodide (BiI_3, 99%), Gamma butyrolactone (GBL, 99.9%), Acetonitrile (ACN) and Methyl acetate (MA), Glacial acetic acid and absolute ethanol were all purchased from Sigma Aldrich, Malaysia.

2.2 Methods

2.2.1 Synthesis of CH_3NH_3I

CH_3NH_3I was synthesized by mixing 27 ml of methylamine (33 wt% in ethanol) and 30 ml of hydroiodic acid (57% in water) and stirred in ice bath at room temperature for 2 h to form a homogeneous solution. The precipitate of CH_3NH_3I was obtained by rotary evaporation at 50° C and then dissolved in ethanol and stirred for 30 min in diethyl ether and then recovered by sedimentation. This step was repeated three times and the white residue of Methylammonium iodide (CH_3NH_3I) was collected and dried at 60°C in a vacuum oven overnight.

2.2.2 Solvent engineering for the synthesis the perovskite films

To synthesize the perovskite film, 160mg of CH_3NH_3I and 590mg of BiI_3 (1:1 ratio) solution were mixed and dissolved in GBL, GBL/ACN (7:3), GBL/MA (7:3) and GBL/ACN/MA (3:1:1) to form the precursor solutions. The resulting solutions were heated at 110°C for 1 h and stirred at 500rpm to obtain homogeneous solutions and then allowed to cool down to room temperature. The precursor solutions were spin-coated on the glass substrate at 1000rpm for 50s, then annealed at 100°C for 10 min. The coated glasses were stored in dark place for photoluminescence characterization. Photoluminescence emission spectra and absorption spectra of the coated glasses were measured using FLS1000 photoluminescence spectrometer.

2.2.3 Synthesis of methylammonium iodobismuthate $(CH_3NH_3)_3Bi_2I_9$ crystals

$(CH_3NH_3)_3Bi_2I_9$ crystals was synthesized as follows: 160mg of CH_3NH_3I and 590mg of BiI_3 was measured in a conical flask and the mixture was ground for 10 min in agar mortar. The resulting mixture was added gradually to 1ml glacial acetic acid solution and simultaneously ultrasonically stirred at 500rpm for 10 min in order to attain homogeneity. The solution was allowed to sediment and the pre-cipitate was collected by filtration, and then washed repeatedly with ethanol in order to remove the residual $(CH_3)_4NI$. The product $(CH_3NH_3)_3Bi_2I_9$ was finally dried at 60°C in a vacuum overnight [11].

2.3 Characterization of $(CH_3NH_3)_3Bi_2I_9$ Crystals

2.3.1 XRD of the synthesized $(CH_3NH_3)_3Bi_2I_9$ crystals

The powder diffraction peaks of $(CH_3NH_3)_3Bi_2I_9$ was carried out using X-ray diffraction (Rigaku Miniflex diffractometer) at an operating voltage of 40 kV and 30mA current, and a scan between a 2θ range of 20–60° with a step size of 0.01.

2.3.2 FESEM/EDS of the synthesized $(CH_3NH_3)_3Bi_2I_9$ crystals

The surface microstructure and morphologies of the samples were studied on a Hitachi FESEM model SU8020 equipment equipped with an electron dispersive spectrum (EDS) accessory which also gives the elemental composition of the synthesized crystal.

2.3.3 Thermal behaviour of $(CH_3NH_3)_3Bi_2I_9$ crystals

The thermal behaviour of $(CH_3NH_3)_3Bi_2I_9$ Crystals as solar cell absorbing layer was characterized using the method described by Juares-Perez, 2016 [12]. The characterization was done using Thermo-Gravimetric Analysis (TGA) and Differential Scanning Calorimetry (DSC).

2.3.3.1 Thermo-Gravimetric Analysis (TGA)

The thermal stability of $(CH_3NH_3)_3Bi_2I_9$ crystal was examined through thermo-gravimetric analysis

(TGA) using thermo-gravimetric analyzer. A 5 mg powder sample of as-produced $(CH_3NH_3)_3Bi_2I_9$ was placed in a sample pan located in furnace of thermo-gravimetric analyzer with a programmable temperature controller. The temperature was increased gradually at a constant rate of 5°C/minute from 30°C to 800°C to incur a thermal reaction for 154 minutes and this was done under Nitrogen gas flow. The thermo-gravimetric data collected from a thermal reaction was compiled into a plot of mass against temperature and time [12].

2.3.3.2 Differential Scanning Calorimetry (DSC)

A sample of $(CH_3NH_3)_3Bi_2I_9$ was placed inside a crucible which was then placed inside a DSC furnace alongside with a reference pan which was emptied. The sample was heated isothermally at the rate of 10°C/min with the temperature range of -50°C – 250°C. The heating and cooling thermograms were recorded for the as prepared sample.

2.4 Determination of Photoluminescence Properties

The photoluminescence spectra of perovskites were determined using photoluminescence spectrometer. $(CH_3NH_3)_3Bi_2I_9$ was deposited on quartz disc using spin coater. After the deposition of $(CH_3NH_3)_3Bi_2I_9$ layer, the film was annealed on a hotplate at 100°C for 5minutes in fume hood. Photoluminescence emission spectra and absorption spectra were measured using FLS1000 photoluminescence spectrometer. The perovskite coated quartz discs were positioned using the face sample holder.

2.5 UV-vis Measurement

The UV-visible measurements of $(CH_3NH_3)_3Bi_2I_9$ were performed using UV3600plus series version 2.52. The powdered sample was scanned with medium speed in the wavelength rang of 300nm to 850nm.

3.0 RESULTS AND DISCUSSION

3.1 Solvent Engineering

To enumerate the photoluminescence (PL) nature of GBL, and GBL enhanced samples, the photoluminescence (PL) spectroscopy of the synthesized perovskites was measured. Figure 1 shows a photoluminescence spectrum of the $(CH_3NH_3)_3Bi_2I_9$ using GBL as solvent. As seen in the emission spectrum, the spectrum exhibits broad emissions within the range of 540 and 588 nm. The spectrum exhibits peaks at 459 and 497 nm. The band gap as seen from the Photograph is calculated as 2.105eV.

Figure 2, 3 and 4 present the PL spectra of the synthesized samples using GBL/ACN, GBL/MA and GBL/ACN/MA respectively. It was observed that the addition of ACN and MA resulted in the reduction of the peaks and efficient quenching. The efficient quenching promotes charge transfer at the perovskite interface resulting in a reduction in the surface charge trapping and efficient charge extraction [13, 14]. From the spectra, it can be seen that there are no changes to the peak emission wavelength in the samples since phase change or thermally induced structures are the possible causes of peak shift. Therefore, the emission spectra are stable with no phase or significant structural changes or distortion.

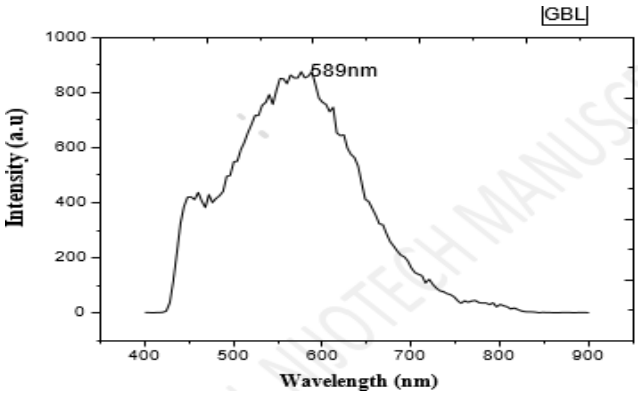

Figure 1: Photoluminescence spectrum of $(CH_3NH_3)_3Bi_2I_9$ with GBL as solvent

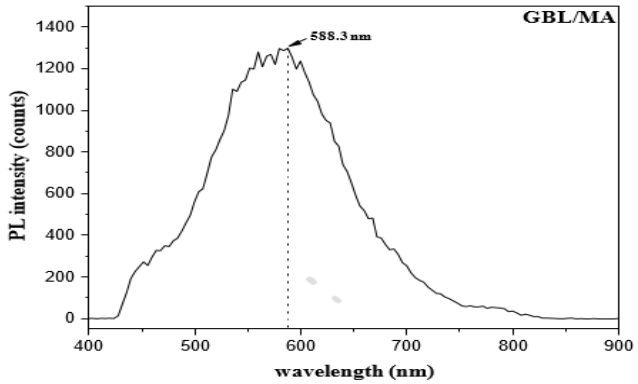

Figure 2: Photoluminescence spectrum of $(CH_3NH_3)_3Bi_2I_9$ with GBL/MA as solvent

The bandgap energy was calculated using the PL spectra. The calculated band gap energy for the solvent engineering is shown in Table 1. The bandgap are 2.105eV for GBL as the solvent, 2.155 eV for GBL/ACN and GBL/ACN/MA and 2.108eV for GBL/MA. It was observed that the bandgap energy

slightly increases with the inclusion of the additives (ACN and MA).

Table 1: Bandgap results of the solvent engineering of $(CH_3NH_3)_3Bi_2I_9$

Sample	Solvent	Volume (%)	Bandgap (eV)
1	GBL	100	2.105
2	GBL/MA	70/30	2.108
3	GBL/ACN	70/30	2.155
4	GBL/MA/ACN	60/20/20	2.155

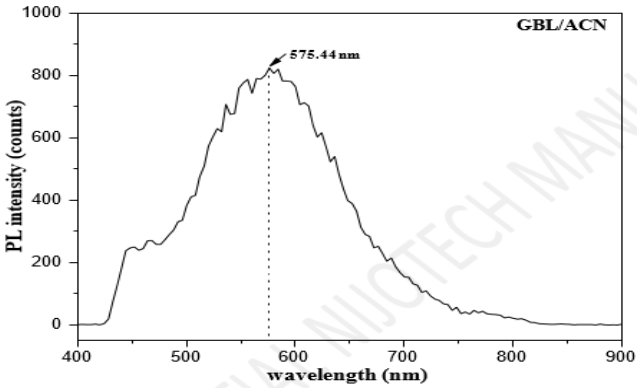

Figure 3: Photoluminescence spectrum of $(CH_3NH_3)_3Bi_2I_9$ with GBL/ACN as solvent

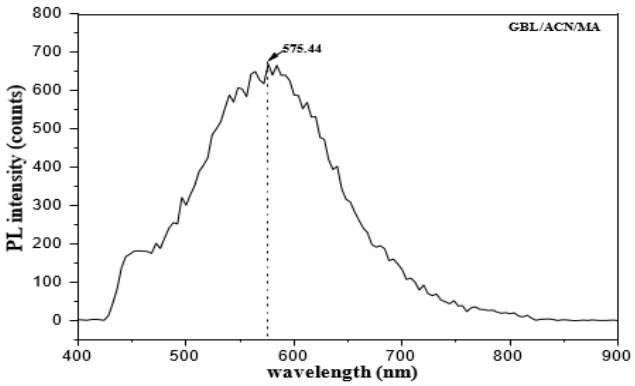

Figure 4: Photoluminescence spectrum of $(CH_3NH_3)_3Bi2I9$ with GBL/ACN/MA as solvent

3.2 XRD of $(CH_3NH_3)_3Bi_2I_9$

The XRD micrograph of the synthesized $(CH_3NH_3)_3Bi_2I_9$ perovskite presented in Figure 5 show two prominent peaks at 2^{θ} = 12.8° and 26.7°. The XRD spectrum showed that the synthesized sample is highly crystalline. The sharp and narrow peaks in the spectrum show that the sample had low average grain size, high crystallinity and effective substitution of the Bismuth ion in the sample. Using the XRD spectrum, the calculated crystallinity was 86% and the average crystallite size was calculated using Scherrer's equation as stated in equation 1.

$$D_A = \frac{K\lambda}{L\cos(\theta)} \quad (1)$$

Where D_A is the average crystallite size, K= dimensionless shape factor (0.9), λ= X-ray wavelength, L = FWHM and θ = Bragg angle. The average crystallite size for the methylammonium bismuth iodide perovskite sample was 35 nm.

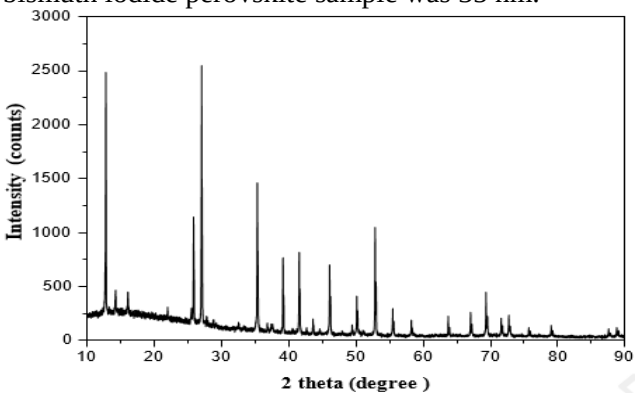

Figure 5: The XRD pattern of the $(CH_3NH_3)_3Bi_2I_9$ perovskite

3.3 FESEM Result of $(CH_3NH_3)_3Bi_2I_9$

Field emission scanning electron microscopy was used to study the surface morphology of the $(CH_3NH_3)_3Bi_2I_9$ and the elements present were identified using the Energy-dispersive spectroscopic technique. Figure 6 show spectrum 1 on the microstructure/FESEM image of $(CH_3NH_3)_3Bi_2I_9$ perovskite. The image contains an irregular shape with pinholes between the grain boundaries. However, the perovskite films had multilayer crystals with disordered orientation resulting in more grain boundaries that might become the traps of charge carriers [15, 16]. The EDS spectrum reveals the presence of I, Bi and C elements in the sample and no impure elements was detected.

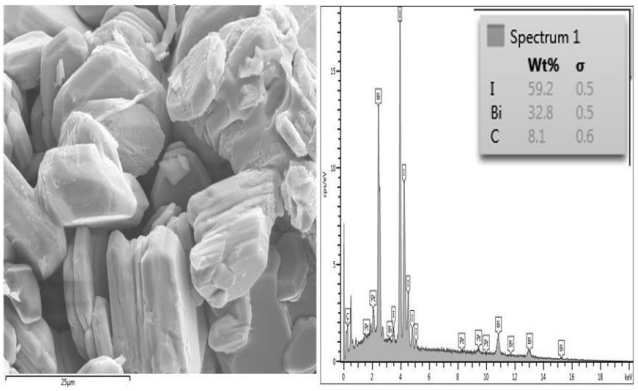

Figure 6: FESEM/EDX image of $(CH_3NH_3)_3Bi_2I_9$

3.4 TGA of the Synthesized $(CH_3NH_3)_3Bi_2I_9$

Figure 7 shows the temperature-dependent weight loss of perovskite. The sample was heated from room temperature to 881°C. In line with general observation, the perovskite sample undergoes

decomposition at 224 ºC resulting in 97.6 % weight loss. This shows that the sample was highly stable since the decomposition started above 220 ºC [14] and no weight loss at the sublimation temperature [16, 17]. The result of this study indicates the thermal stability of the $(CH_3NH_3)_3Bi_2I_9$ perovskite sample for the intended application.

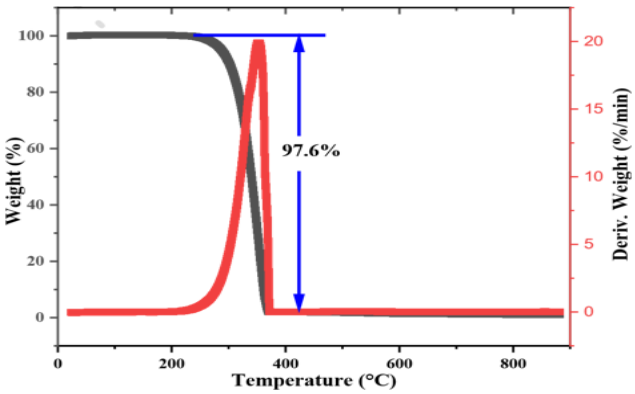

Figure 7: The Thermogravimetric Analysis and derivative weight of the $(CH_3NH_3)_3Bi_2I_9$ perovskite

3.5 DSC of the Synthesized $(CH_3NH_3)_3Bi_2I_9$

The DSC result of the synthesized $(CH_3NH_3)_3Bi_2I_9$ is shown in Figure 8, the curve exhibits endothermic peaks during the heating processes. The first peak at 94.2ºC is an endothermic peak attributed to the total removal of OH content in the sample. The sharp and wide hysteresis peak at 165ºC reveals the first-order phase transition. From the curve, the perovskite is thermally stable up to 230ºC.

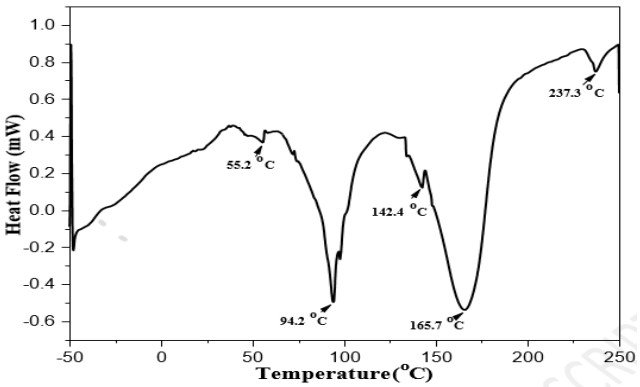

Figure 8: Differential Scanning Calorimetry for $(CH_3NH_3)_3Bi_2I_9$

3.6 UV vis Measurement Result of $(CH_3NH_3)_3Bi_2I_9$

Figure 9 shows the UV Vis spectrum of the $(CH_3NH_3)_3Bi_2I_9$. The spectrum had three strong absorptions at 360 nm, 576 nm and 670 nm and the absorption band was used to calculate the optical absorption coefficient (α) based on the Kubelka-Munk equation. Using the Equation, the optical energy bandgap was determined to be 1.58 eV as calculated from the Tauc fit. The optical band gap obtained in the study is similar to the literature [18]. The PL band of the $(CH_3NH_3)_3Bi_2I_9$ thin-film perovskite solar cells initiate from a near band edge transition is 1.58 eV.

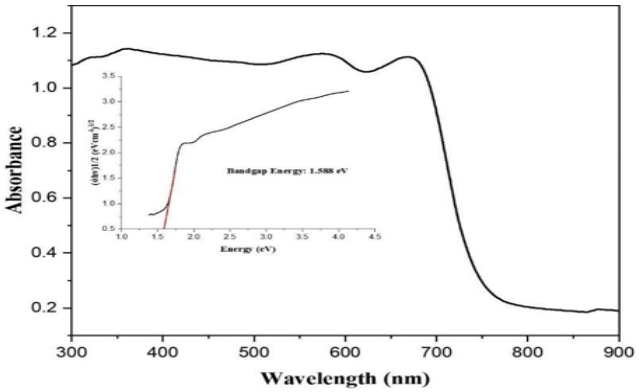

Figure 9: UV−vis spectroscopy spectrum of methylammonium bismuth iodide associated with a Tauc plot analysis.

4.0 CONCLUSION AND RECOMMENDATION

4.1 Conclusion

With keen interest in research in the field of solar cell as an alternative clean energy source to erratic power generation/supply in my country (Nigeria), the researcher has synthesized and characterized a lead-free light absorbing layer OIHP solar cell application via solvent engineering and hence characterized it for solar cell application. Based on the results achieved in this research work, the following conclusions had been drawn out.

Firstly the synthesized $(CH_3NH_3)_3Bi_2I_9$ perovskite was thermally stable for solar cell application as it requires very high temperature (> 220ºC) for its degradation to be noticed. Secondly, the bandgap of $(CH_3NH_3)_3Bi_2I_9$ is 1.5eV which is within an ideal band gap for solar cell active layer material (1.5-1.6eV). The result of the band gap can be attributed to the band gap solvent engineering for the synthesis.

4.2 Recommendation

More instigation into the synthesized techniques for the material is needed as this can hopefully improve on its performance to meet world class demand for green energy generation.

REFERENCES

[1] Bagher, A. M, Vahid, M. M. A, and Mohsen, M. "Types of solar cells and application", *American Journal of Optics and Photonics* 3(5): 94-113; 2015.

[2] Xing, G., Mathews, N., Sun, S., Lim, S. S., Lam, Y. M., Graẗzel, M., Mhaisalkar, S., Sum, T. C. "Long-range balanced electron-and hole-transport lengths in organicinorganic CH3NH3PbI3", *Science* 342 (2013) 344–347, https://doi.org/10.1126/ science.1243167.

[3] Ding, C., et al. "Effect of the conduction band offset on interfacial recombination behavior of the pl*anar perovskite solar cells", Nano Energy*; 2018.

[4] Zhou, H. P., Chen, Q., Li, G., Luo, S., Song, T. B., Duan, H. S., Hong, Z. R., You, J. B., Liu, Y. S., and Yang, Y. "Interface engineering of highly efficient perovskite solar cells", *Science*, 2014; 345:542–546

[5] Dong, Q., Fang, Y., Shao, Y., et al. "Solar cells. Electron-hole diffusion lengths > 175 μm in solution-grown CH3NH3PbI3 single crystals", *Science 347*, 2015; https://doi.org/ 10.1126/science.aaa5760, 967–70.

[6] Shi, D., Adinolfi, V., Comin, R., Yuan, M., Alarousu, E., Buin, A., Chen, Y., Hoogland, S., Rothenberger, A., Katsiev, K., Losovyj, Y., Zhang, X., Dowben, P. A., Mohammed, O. F., Sargent, E. H., and Bakr, O. M. "Low trap-state density and long carrier diffusion in organolead trihalide perovskite single crystals", *Science 347*, 2015; 519–522, https://doi.org/10.1126/science.aaa2725.

[7] Lian, Z., Yan, Q., Gao, T., Ding, J., Lv, Q., Ning, C., Li, Q., and Sun, J. L. "Perovskite $CH_3NH_3PbI_3$(Cl) single crystals: rapid solution growth, unparalleled crystalline quality, and low trap density toward 108 cm-3", *J. Am. Chem. Soc. 138*, 2016; 9409–9412, https://doi.org/10.1021/jacs.6b05683.

[8] Tsutomu, M., Kojima, A., Teshima, K., Shirai, Y. "Organometal Halide Perovskites as Visible-Light Sensitizers for Photovoltaic Cells", *Journal of the American Chemical Society*, 2009; 131(17):6050-1DOI: 10.1021/ja809598r

[9] Stranks, S. D., Eperon, G. E., Grancini, G., Menelaou, C., Alcocer, M. J. P., Leijtens, T., Herz, L. M., Petrozza, A., and Snaith, H. J. "Electron-hole diffusion lengths exceeding 1 micrometer in an organometal trihalide perovskite absorber", *Science 342*, 2013; 341–344, https://doi.org/10.1126/science.1243982.

[10] Minemoto, T., et al. "Theoretical analysis on effect of band offsets in perovskite solar cells Sol". *Energy Mater. Sol. Cells*, 2015.

[11] Jia, X., Hu, Z., Zhu, Y. "Facile synthesis of organic–inorganic hybrid perovskite $CH_3NH_3PbI_3$ microcrystals, *Journal of Alloys and Compounds 725*, 2017; DOI:10.1016/j.jallcom.2017.07.154

[12] Juarez-Perez, E. J., Hawash, Z., Raga, S. R., Ono, L. K., and Qi, Y. "Thermal degradation of $CH_3NH_3PbI_3$ perovskite into NH_3 and CH_3I gases observed by coupled thermogravimetry–mass spectrometry analysis". *Energy & Environmental Science*, 2016; 9(11), 3406–3410. doi:10.1039/c6ee02016

[13] You, J., Hong, Z., Yang, Y., Chen, Q., Cai, M., Song, T. B., Chen, C. C., Lu, S., Liu, Y., Zhou, H., and Yang, Y. "Addressing the stability issue of perovskite solar cells for commercial application" *ACS Nano 8*, 2018:1674–1680

[14] Liu, Y., Yang, Z., Cui, D., Ren, X., Sun, J., Liu, X., and Liu, S. "Two-inch-sized perovskite $CH_3NH_3PbX_3$ (X= Cl, Br, I) crystals: growth and characterization". *Advanced Materials*, 2015; 27(35), 5176-5183.

[15] You, J., Hong, Z., Yang, Y., Chen, Q., Cai, M., Song, T. B., Chen, C. C., Lu, S., Liu, Y., Zhou, H., and Yang, Y. "Low-temperature solution-processed perovskite solar cells with high efficiency and flexibility", *ACS Nano 8*, 2014:1674–1680

[16] Zhao, D., Tang, Y., Song, B., Guo, J., and Hou, Y. "The Trapped Charges at Grain Boundaries in Perovskite Solar Cells", *Advanced Functional Materials*, 2021; 31(49), 2107125.

[17] Zhou, J., Xia, Z., Molokeev, M. S., Zhang, X., Peng, D., and Liu, Q. "Composition design, optical gap and stability investigations of lead-free halide double perovskite $Cs_2AgInCl_6$. *Journal of Materials Chemistry A*, 2017; 5(29), 15031-15037.

[18] Baikie, T, Y., Fang, J. M., Kadro, M., Schreyer, F., Wei, S. G., Mhaisalkar, M., Graetzel, T. J. and White. "Synthesis and crystal chemistry of the hybrid perovskite (CH_3NH_3) $sPbI_3$ for solid-state sensitised solar cell applications", *J. Mater. Chem. A. 1*, 2013; 5628, https://doi.org/10.1039/c3ta10518k.